Microstructural and in vitro characterisation of 45S5 bioactive glass coatings deposited by Solution Precursor Plasma Spraying (SPPS)

E. Cañas [a,*], M.J. Orts [a], A.R. Boccaccini [b], E. Sánchez [a]

[a] Instituto de Tecnología Cerámica (ITC), Universitat Jaume I (UJI), 12006, Castellón, Spain

[b] Institute of Biomaterials, University of Erlangen–Nuremberg, 91058, Erlangen, Germany

Eugeni Cañas Recacha Telephone number: (+34) 964342424

Email: eugeni.canas@itc.uji.es Fax number: (+34) 964342425

María José Orts Tarí

Email: mariajose.orts@itc.uji.es

Aldo R. Boccaccini

Email: aldo.boccaccini@fau.de

Enrique Sánchez Vilches

Email: enrique.sanchez@itc.uji.es

Abstract

The present work focused on the development of bioactive glass coatings employing Solution Precursor Plasma Spraying. Precursors of SiO_2, CaO, Na_2O and P_2O_5 were mixed in distilled water to prepare concentrated solutions with a composition close to the 45S5 bioactive glass. Solutions were rheologically characterised to assess their stability with time and deposited onto AISI type 304 stainless steel to develop coatings under different parameters related to the thermal spraying technique. The effect of these parameters on coatings microstructure was studied by scanning electron microscopy. Coatings were also analysed by X–ray diffraction and scratch test to complete the microstructural characterization. Moreover, coatings bioactivity was evaluated by immersing them in Simulated Body Fluid.

The study showed that using short spraying distances and low argon flow rates, gave rise to the typical microstructure derived from liquid feedstocks whereas some crystallization associated to the long spray distance used occurred. Scratch test revealed that the resulting coating possessed good mechanical properties when compared with similar coatings obtained by other plasma spraying techniques. Moreover, the obtained coating could develop an hydroxycarbonate apatite layer when in contact with Simulated Body Fluid as demonstrated by scanning electron microscopy, X–ray diffraction and Fourier transform infrared spectroscopy.

Keywords: Bioactive glass solution; Solution stability; Solution precursor plasma spraying; Scratch test; In vitro test

1. Introduction

Bioactive materials were developed as an improvement with regard to the bioinert materials typically used in the field of medicine [1,2]. The most studied bioactive material, which has been used for long time, is hydroxyapatite. This biomaterial is employed in a wide range of medical applications [3–5].

Not long ago, Prof. Hench discovered by accident a glass material composed of a silicate network incorporating sodium, calcium and phosphorus (45% SiO_2, 24.5% CaO, 24.5% Na_2O and 6% P_2O_5, in wt%) [6,7]. This glass, known as Bioglass® or 45S5 bioactive glass, has proved to be more bioactive and to possess better osseointegration than hydroxyapatite [8,9], so that it can be used in different clinical treatments such as periodontal disease, bone regeneration or in middle ear surgery [7,10–12]. In addition, the US Food and Drug Administration (FDA) approves its employment in medical applications [7].

The main disadvantage of this material is its brittleness, which limits its utilisation in load–bearing applications [13,14]. To solve this problem, researchers started to develop the deposition of bioactive glass onto metallic substrates developing a composite layer which combines good mechanical properties with high bioactivity. Different techniques have been studied to deposit this type of coatings, i.e. enamelling, glazing, magnetron sputtering and pulsed laser deposition [15–19]. Among all these techniques, plasma spraying is the most employed method due to the high deposition rate, the good control of the substrate degradation (compared to the other deposition techniques) and the possibility of controlling the morphology, thickness and structure of the coating, and therefore its properties [15]. In addition, plasma spraying gives the chance of easily producing dense coatings which are suitable to be scaled–up for implantable devices.

Typically, plasma sprayed coatings have been deposited using glass powder. These powders can be obtained either by the melting and quenching method or by the sol–gel method accompanied by subsequent thermal treatment [20, 21].

Literature shows that bioactive glass coatings from powder feedstocks with good bioactivity can be deposited by plasma spraying. However, the coatings exhibited a cracked, highly porous microstructure with poor adhesion to the substrate [20, 22].

Recently, the employment of liquid feedstocks such as suspensions and solutions instead of powder feedstocks has received great interest in the thermal spray community for different materials, due to the unique coating properties achieved, whereas thinner (40–50 μm) submicron– to nano–sized coatings could be easily produced [23–27].

For the case of bioactive glass coatings, its deposition from suspension feedstocks has been recently addressed. Thus, reported findings showed that final coatings displayed similar microstructures to those obtained from powder feedstocks [8, 28, 29]. On the contrary, the utilisation of solution feedstocks in the development of glass coatings has been hardly investigated while significant advantages can be obtained. On the one hand, thinner and nanostructured coatings with a more homogeneous microstructure can be engineered. On the other hand, using solutions allows to work with pure feedstocks comparing to powders and suspensions, since the preparation of both feedstocks implies a series of laborious steps which can often introduce some contaminants in the working material.

In a previous work, the authors presented a preliminary study on the possibility of obtaining bioactive coatings using solution precursor plasma spraying (SPPS) [30]. Therefore, this current work aims to complete the previous research by determining the stability of the solution feedstocks as well as analysing their thermal behaviour inside the plasma torch. In addition, the effect of the employed spraying parameters on the morphology of the coatings was investigated. A mechanical characterization by scratch technique was carried out on bioactive glass coatings obtained by plasma spray for the first time. Finally, a complete study of the coatings bioactivity was developed for long soaking times.

2. Experimental

2.1. Preparation of the solution feedstock

Following the previous work [30], bioactive glass 45S5 was selected as the working composition. Solutions were prepared with a precursor concentration of 4 M (4 moles of precursors per litre of solution), using water as a solvent. The reactants listed below were used to synthesise the solution feedstock:

- Tetraethyl orthosilicate or TEOS ($C_8H_{20}O_4Si$ synthesis grade, Merck, Germany) as a source of SiO_2.
- Triethyl phosphate or TEP ($C_6H_{15}O_4P$ synthesis grade, Merck, Germany) as a source of P_2O_5.
- Calcium nitrate ($Ca(NO_3)_2{\cdot}4H_2O$ >99%, VWR Chemicals, USA) as a source of CaO.
- Sodium nitrate ($NaNO_3$ >99%, Sigma–Aldrich, USA) as a source of Na_2O.

Those precursors were chosen basing on literature related to the development of 45S5 bioactive glass employing the sol–gel method [31–33]. Nevertheless, both alkoxides (TEOS and TEP) are not miscible in water, therefore it is necessary to add a catalyst in order to hydrolyse them [30]. Although there are different types of catalysts for that purpose, nitric acid is the most used one [32–34]. Higher amounts of catalyst drastically increase the gelation velocity of the sol. However, it is well known that the higher the nitric acid concentration, the lower the glass particle size [31]. Consequently, if the amount of catalyst is varied in the solution feedstock, glass particles with different sizes will be formed inside the plasma torch. For that reason, in the present work, the concentration of nitric acid (HNO_3, Tritripur, Merck, Germany) used in the solution feedstocks was 1, 0.5 and 0.2 M (where the latter is the same as in the previous study [30]). The concentrations of catalyst are in moles of nitric acid per litre of water. The solution without catalyst was discarded since in the previous work [30] no coating was obtained when this feedstock was used.

The procedure followed to prepare the feedstocks was the one used in the preliminary work [30], and involved mixing the distilled water and nitric acid to achieve an acidic dissolution. Then, TEOS was slowly added to the dissolution under magnetic stirring with a molar ratio water to TEOS of 18. After that, the mixture was kept in agitation during 30 minutes until full clarification. The amount of the remaining reactants was deduced from 45S5 glass composition by stoichiometry. TEP was added in the same way as the TEOS, keeping the mixture under stirring for another 30 minutes. Finally, calcium and sodium nitrates were added to the mixture under stirring, keeping the agitation for an additional hour. Finally, the solution feedstocks were kept at a temperature of 5 ºC inside a sealed container, unlike how it was done previously [30], where the solutions stayed at room temperature overnight, since the stability of the sols could be highly improved by cooling them [35].

2.2. Characterization of the feedstock

Once all the solution feedstocks were synthesised, their chemical compositions were determined by wavelength dispersive X–ray fluorescence spectrometry (XRF) (AXIOS, PANalytical, The Netherlands). To carry out this test, a powder sample was obtained from each solution feedstock by drying the solution in a stove at 100 ºC and subsequent thermal treatment in an electric furnace at 700 ºC. Then, the resulting powder was dry milled and fused into beads for XRF using a Panalytical PERL'X 3 bead maker. Chemical composition was assessed in the above mentioned XRF spectrometer provided with a Rh anode tube. Certified reference materials were used to guarantee the measurement traceability.

On the other hand, the thermal behaviour of the developed sols was examined by both differential thermal analysis and thermo–gravimetric analysis (DTA–TG) in order to understand the processes which occurred to the feedstocks during the spraying [36]. DTA–TG tests were done in a thermal analyzer (TGA/SDTA 851e, Mettler Toledo, Switzerland) putting each solution sample without drying it inside a platinum crucible and heating the material

from room temperature up to a maximum temperature of 1200 °C in air, employing a heating rate of 10 °C min^{-1}.

In addition, as different amounts of catalyst were used, the stability with time (or the gelation time) of each feedstock was assessed through a rheological characterisation at different times using a rheometer (CVO 120, Bohlin Instruments, Great Britain) which controlled the shear rate (CR). The test was carried out at room temperature (298 K) using a double–gap system in which the shear rate was loaded from 0 to 500 s^{-1} in 5 min, maintained at 500 s^{-1} for 1 min and downloaded from 500 to 0 s^{-1} in 5 min.

2.3. Coatings deposition

The bioactive glass coatings were deposited by solution precursor plasma spraying (SPPS). The thermal spraying facility comprised a mono–cathode plasma torch (F4–MB, Oerlikon Metco, Switzerland), coupled to a six–axis robot (IRB 1400, ABB, Switzerland). Argon was used as primary plasma gas and hydrogen as secondary plasma gas. The torch was connected to a home–made liquid feeding system, which injected the liquid feedstock in a radial way by mechanical injection. Details about the facility have been reported in previous works [37, 38]. The glass coatings were sprayed onto AISI type 304 stainless steel discs with a diameter of 25 mm. Before coatings deposition, the substrates were grit–blasted using black corundum with a pressure of 4.2 bar and cleaned with ethanol in an ultrasonic bath. The roughness (R_a) of the substrates after the grit–blasting step was measured employing a roughness measurement equipment (Hommelwerke T8000, Jenoptik AG, France), obtaining a R_a value of 2.2 ± 0.1 µm. In addition, prior to glass coating deposition, a bond coat was sprayed from anatase feedstock (Metco 102, Oerlikon Metco, Switzerland) with a particle size distribution ranging from 10 to 55 µm by atmospheric plasma spraying (APS), with the aim of enhancing the top coating adhesion [39]. The parameters used to deposit the bond coat, given by the supplier, are showed in table 1.

Finally, the solution feedstocks were deposited employing the facility described above, and preheating the substrates between 300 °C and 350 °C. The spraying conditions utilised in this work are also detailed in table 1, which correspond to that used in the previous work [30]. As it can be seen, two different spraying distances and argon flow rates (giving rise to different plasma torch energy) were used, in order to find the optimal parameters for the deposition. The variation of these two variables was since they strongly affect the final microstructure of the coating as previously reported [40, 41].

2.4. Coatings characterization

In order to evaluate the effect of the spraying parameters on the morphology of the coatings, the coatings were metallographically prepared by cutting and polishing. Surfaces and polished cross–sections of the coatings were observed in a field–emission gun environmental scanning electron microscope (FEG–ESEM) (QUANTA 200FEG, FEI Company, USA) with the backscattered electron detector signal.

Moreover, the nature of the phases (amorphous or crystalline) of the as–sprayed coatings was determined by X–ray diffraction (XRD) (Theta–theta D8 Advance diffractometer, Bruker, Germany) over a range of 2θ between 10º and 80º, with the difference that the detector used (VANTEC–1) had higher resolution than that used in [30].

On the other hand, the adhesion of the coatings has been evaluated. Since coatings from liquid feedstocks, specially from solutions, typically showed thin thicknesses, it is not possible to employ the normalized tensile test (ASTM–C633) to determine this property. Therefore, in this work, the scratch test was chosen in order to determine the final coatings adhesion [42]. For that purpose, a scratch tester (Revetest, CSM Instrument, Germany) equipped with a conical diamond Rockwell indenter of spherical tip with a radius of 200 µm was used. Scratches of 1 cm length were made in each sample tested, progressively increasing the load applied from 0 to 10 N. To avoid errors caused by the presence of specific defects on the

sample surface, three scratches were made on each sample. Before and after scratching, the indenter went through the tested area applying a minimum load and registering the original profile of the surface, with the aim of detecting changes in depth experienced by the scratched area. In addition, an optical microscope was coupled to the equipment, which allowed the visual characterisation of the changes in the scratching mechanism by taking micrographs of the scratches made in each sample. The critical load was determined as the force at which the bond coating started to be visible. The scratch hardness was also determined from equation (1) and related to the cohesion of the coating.

$$HS_P = \frac{k \cdot P}{w^2} \quad (1)$$

where HS_P is the scratch hardness (GPa), P is the applied force (grams–force), k is a geometrical constant (24.98) and w is the scratch width (μm).

2.5. In vitro test

In vitro test of the coatings was performed following a standard protocol of soaking in Simulated Body Fluid (SBF) [43].

First, the needed amount of SBF was prepared following the method of Professor Kokubo [44]. Then, the coatings were soaked in SBF inside a plastic vessel, using a fix volume of SBF determined by equation (2).

$$V_{SBF} = \frac{S_c}{10} \quad (2)$$

where V_{SBF} is the volume of SBF (in mL) and S_c is the area of the glass coating (mm^2). For the present study, as disks substrates with 25 mm diameter were used, coatings with an area of 490 mm^2 were obtained, and hence 49 mL of SBF were used for each coating sample. Sometimes, hydroxycarbonate apatite (HCA) can precipitate in the SBF and be deposited on the surface of the coating, giving rise to fake results [44]. To avoid that, in this test the samples were placed inside the vessel in such a way that the coating was perpendicular to the

bottom surface of the container. The vessels containing the coatings in SBF were placed inside a water bath at 36.5 ± 0.5 ºC. Coatings were tested for 1, 7 and 14 days. After each soaking time, the pH of the SBF was measured and the coated sample was removed from the vessel and gently washed with distilled water. After that, the as–soaked coatings were coated with a very thin platinum layer in order to observe their surface morphology by FEG–ESEM using the secondary electron detector signal.

In addition, the nucleation and growth of HCA was monitored for each soaking time. For that purpose, the chemical composition of the surface of the as–soaked coatings was determined by an energy–dispersive X–ray microanalysis instrument (Genesis 7000 SUTW, EDAX, USA) coupled to the FEG–ESEM. XRD, over a range of 2θ between 10º and 80º, and Fourier transform infrared spectroscopy (FTIR) (Nicolet 6700, Thermo Scientific, USA) in absorbance mode with a spectral resolution of 2 cm^{-1} from 1500 to 500 cm^{-1} were also carried out.

3. Results and discussion

3.1. Bioactive glass solutions characterization

The obtained solution feedstocks showed a composition very close to that of the 45S5 bioactive glass (Table 2). No significant differences between the solutions containing different amount of catalyst were found since all of them were made from the same amount of each precursor.

Concerning the DTA–TG analysis, the results are represented in figure 1. It can be seen that the three feedstocks displayed a similar behaviour, since the same amount of precursors was used in the preparation of each sol as explained above. The same endothermic and exothermic peaks were observed in all cases, which suited well with those reported in the literature [33]. At 100 ºC there was an endothermic peak which corresponds to the water removal. This stage was accompanied by a 60 % weight loss (as the TGA graphs show). Then, at about 235 ºC there was another endothermic peak which could correspond to the elimination of more water, resulting from condensation of precursors and catalyst. In all cases, the weight loss was around 5%. After that, in the range of 600–800 ºC, both endothermic and exothermic peaks could be found. Moreover, two endothermic peaks (600 and 700 ºC approx.) are visible, which correspond to the elimination of nitrates from the sodium and calcium precursors, and one exothermic peak (750 ºC approx.) is visible, which might be attributed to glass crystallization. These steps are accompanied by 15% weight loss. An 80% weight loss was observed in the entire performed cycle for all the feedstocks.

The flow curves of the three solution feedstocks are shown in figure 2. Each curve corresponds to a solution with a different concentration of catalyst, and all of them were determined immediately after the preparation of each feedstock. As the catalyst content increases the viscosity of the feedstocks also augments, but in general all feedstocks display very low viscosity (quotient between the shear stress and the shear rate). On the other hand, all curves present a slope change for a shear rate between 150 and 200 s^{-1}. It is well known

that solution precursors show a newtonian liquid behaviour, but in this case the resulting curves display a slight shear–thickening behaviour. This apparent anomaly, which is usually observed in sol–gel solutions with low viscosity, is caused by a slippage effect [45].

Apart from this, a priori all feedstocks were appropriate to be sprayed since they showed a similar and proper thermal behaviour in the plasma torch leading to melted glass. In addition, solutions were suitable to be transported through the plasma facility pipes and subsequently injected into the plasma torch since they had low viscosity at high shear rates.

However, if a further study of feedstock solution viscosity (at 500 s^{-1} shear rate) was carried out over time, it could be appreciated that not all feedstocks are appropriate to SPPS process, as shown in figure 3. As expected, higher amounts of catalyst gave rise to high gelation velocity. Thus, only in ten hours, the solution with 1 M nitric acid showed a dramatic increase of viscosity, which proved that the solution had completely gelled leading to a densified gel. The 0.5 M catalyst solution presented a similar behaviour to that of the 1 M solution. It took more time to this feedstock to become a densified gel, but after 1 day the nucleation of gel agglomerates began inside the feedstock, which could clog the nozzle. In contrast, the solution with 0.2 M nitric acid showed a different behaviour. As it can be seen in figure 3, the gelation process took place very drastically, although it needed between 7 and 9 days to occur. Results obtained from these tests revealed the high stability of 0.2 M catalyst solution, while the solutions prepared with 1 and 0.5 M of catalyst possessed very low stability with time.

3.2. Microstructural characterization of bioactive glass coatings

Due to the very low stability presented by the solution feedstocks with a catalyst concentration of 1 and 0.5 M, as seen in the previous section, these were discarded in order to avoid clogging of both the pipes and the injector. Only the solution with 0.2 M of catalyst was sprayed using the parameters of table 1. Combinations of spraying distance and argon flow rate resulted in an experimental grid composed of 4 different tests as showed in table 3.

The surface micrographs of the obtained coatings from the 0.2 M catalyst solution feedstock (runs 1 to 4) are showed in figure 4 at different magnifications. All experiments led to uniform coating surfaces, but the morphology of each surface was completely different because of both the spraying distance and the argon flow rate used. Coating from experiment 4 (Figures 4d and 4h), i.e. high spraying distance and low argon flow rate, displayed the worst microstructure of the 4 tests carried out with the 0.2 M catalyst feedstock. The whole coating was composed of very fine rounded glass particles loosely connected with each other, similar to the "powdery deposits" named by L. Xie et al. [46], and poorly attached to the substrate since they were easily removed from it. Coating deposited employing the parameters of test 2 (Figures 4b and 4f), i.e. high spraying distance and high argon flow rate, presented a similar microstructure than that of the 4–test coating, but the employment of higher enthalpy gave rise to the formation of some isolated glass agglomerates. Even so, most of the coating was formed by powdery deposits, resulting in a coating with an impaired adhesion.

Contrary to those tests (experiments 2 and 4), conditions operated in experiments 1 (Figure 4a and 4e) and 3 (Figures 4c and 4g), i.e. short spraying distance and two different argon flow rates, led to good coatings featured by denser and more homogeneous surfaces showing the two–zones microstructure typical of liquid feedstock deposition, i.e. a first layer of fine glass rounded drops followed by a top layer of larger glass agglomerates. This type of microstructure was developed due to the high precursor concentration of the employed feedstock [36]. Although both experiments were carried out under the same spraying distance, the glass agglomerates of the top zone were highly influenced by the plasma energy which varied in function of the argon flow rate. For the coating of run 1, these agglomerates were coarser and appeared more melted, splashed and cohesive due to the greater amount of energy received from the plasma plume throughout the deposition process. For the run 3, the agglomerates looked smaller and more isolated than those of experiment 1. In addition, their morphology was much rounded, evidencing the low melting and splashing degree of the

agglomerates and probably their poor adhesion to the substrate. To summarize, four different coatings were deposited employing the solution containing 0.2M of nitric acid. It was found that, regardless the argon flow rate employed, higher spraying distances resulted in coatings made up of powdery deposits without adhesion to the coating, while for shorter spraying distances an energetic plasma plume derived from the use of low rates of argon, led to well adhered coatings comprising quite molten and splashed particles.

In fact, cross–section characterisation was only successfully accomplished for the coating deposited under parameters of run 1, since it was the only coating that presented a minimal adhesion to remain on the substrate after the metallographic preparation step. The resulting micrographs are presented in figure 5 at different magnifications. As observed, the resulting coating displayed a dense and homogeneous microstructure with and average thickness of approximately 35 μm consisting of very fine re–solidified spherical glass drops entrapped in a molten glass matrix. In addition, the coating showed an open and interconnected porosity, which could improve the reaction ability of the coating with biological fluids, since the surface area is expected to be high.

On the other hand, XRD analysis of this coating (experiment 1) is presented in figure 6. In the preliminary work done by the authors [30], the XRD pattern revealed not only a predominant amorphous phase, but also a succession of peaks corresponding to the anatase layer sprayed as bond coat. Nevertheless, as a new X–ray detector with higher resolution was used, under these new conditions the XRD pattern also displayed crystalline peaks corresponding to combeite. This material is a sodium and calcium silicate which crystallises from the 45S5 bioactive glass [20]. The formation of this crystalline phase may be due to the long spraying distance utilised, which allowed some of the glass molten drops that fly in the peripheral area of the torch to re–solidify and crystallise before impacting to the substrate giving rise to the formation of crystalline spheres [47, 48]. Then, these spheres were trapped by the softer or melted drops. In addition, the XRD pattern also exhibited one peak corresponding to

tricalcium silicate (Ca_3SiO_5), which resulted from the reaction between 3 moles of calcium oxide with 1 mole of silicon dioxide. The presence of these crystalline phases could reduce the bioreactivity of the developed coating.

3.3. Scratch test results

Scratch test was carried out on the resulting coating from run 1, following the procedure described in section 2.4. For the sake of comparison, the test was also done on 45S5 bioactive glass coatings deposited by atmospheric plasma spraying (APS) and suspension plasma spraying (SPS). The APS coating was the one called BGGS4 from ref. [20], but sprayed onto TiO_2 bond coating. The SPS coating was the one shown in ref. [8], sprayed under 70 mm spraying distance. The three coatings were deposited using the same number of torch passages, that is 5.

The obtained mechanical parameters (critical load and scratch hardness) are shown in table 4.

For the SPS and SPPS coatings, the scratch hardness was calculated with the critical load while for the APS coating this parameter was determined with the maximum applied force. Figure 7 shows an optical micrograph of one scratch performed in the tested coatings. An example of the penetration depth curve is plotted in figure 8.

The APS coating showed a critical load (L_c) higher than the maximum force applied (10 N), therefore it is not possible to visualize the bond coating probably due to the great thickness of this coating. In addition, it can be seen in figure 8a that the penetration of the tip is quite deep, owing to the higher thickness. Therefore, the adhesion of this coating could not be as good as would be expected. Moreover, the scratch hardness value lies between those of the SPS and SPPS samples, since this coating presents a microstructure containing numerous closed pores which reduce the contact between splats [20], impairing the cohesion of the coating. The deeper penetration of the tip into the coating as well as the large width of the scratch shown in

figure 7a confirm the poor cohesion of this coating. Moreover, as appreciated in this figure the splats have been ripped off and dragged by the tip.

Concerning the SPS coating, this coating presents the worst adhesion and cohesion behaviour of all coatings investigated. The critical load (L_c) and the scratch hardness are very low. Although the penetration depth of the tip appears quite regular, the scratch width is very high (higher than that of the APS coating). In figure 7b it can be seen that tearing and delamination of the coating occurred around the scratch, and the coating is dragged until the end of the tip travel, similarly as in the APS coating, but to a larger extent. This behaviour is due to the microstructure of the coating; as reported in the previous study [8], the coating is composed of two layers, a first one of fine and rounded glass drops sintered between them and a top layer made up of coarse glass agglomerates poorly attached to the first layer, being these agglomerates the ones that were delaminated and dragged.

On the contrary, despite the intermediate value of the critical load (L_c) which demonstrated a regular adhesion, the SPPS coating deposited in the present work showed the best cohesive mode, as deduced by its highest scratch hardness shown in table 4. In fact, from figure 7c, it can be observed that the scratch width is much narrower than those performed on the other coatings. In addition, as it can be seen in Figure 8c, the penetration path of the tip is regular and homogeneous. It can be concluded that the coating obtained from run 1 of the present work possessed good structural integrity when compared with its APS and SPS coating counterparts.

3.4. In vitro test results

The in vitro test was performed on the coating from experiment 1 since this coating showed enough adherence to the substrate to be characterized.

The variation of the SBF pH in function of the soaking time is showed in figure 9. A control sample (only SBF without coating) was also checked. Although the pH of the control sample

remained constant over time, the pH of the SBF sample containing the coating underwent a significant increase, so that a reaction occurred between the incubating medium and the glass coating [43]. This increment in pH was very marked during the first day of incubation, becoming more progressive through the next 2 weeks of incubation. However, the final pH reached was low, evidencing that the crystalline phases founded in the coating negatively affected its bioreactivity.

Then, the reaction between the coating and the SBF was confirmed by SEM. Figure 10 shows surface micrographs from SEM observation. For each soaking time, a global surface micrograph was presented followed by one of each zone of the coating (first layer and top agglomerated layer) at higher magnifications. Figure 10a shows the coating after 1 day of immersion in SBF, where the large agglomerates of the top layer seemed to have started to dissolve in the reaction medium, as they look smaller than those showed in figure 4a being this fact part of the steps which took place during the soaking test. At higher magnification (Figures 10b and 10c), in the coating soaked for 1 day it could be observed that the first layer of the coating had reacted and had been covered with HCA, while the agglomerates of the upper layer, even though they were partially dissolved, hardly showed presence of HCA, only isolated areas of the surface of these agglomerates appeared reacted. This difference in the reaction rate deals basically with the different sizes between the agglomerates and the fine glass particles of the first layer, which displayed a much higher surface area. For 7 days, it can be seen how the agglomerates in the top layer became more dissolved (Figure 10d), as well as they showed a continuous layer of HCA (Figure 10e) and the first layer of glass was totally reacted and fully covered with this material (Figure 10f). Finally, after 14 days in SBF, no further dissolution of the glass took place (Figure 10g), since the surface appearance was similar to that of the coating immersed for 7 days. However, for 14 days in SBF, both zones of the coating (the top zone and the first glass layer) appeared completely reacted and covered

with HCA (Figures 10h and 10i). Even so, the first layer was always more reacted than the agglomerates.

The aforementioned behaviour was confirmed by EDX analysis. As it can be seen in figure 11a, the intensity of the P and Ca peaks corresponds to 45S5 bioactive glass. However, with higher soaking times (Figures 11b, 11c and 11d), the P and Ca peak intensities increased, which evidenced the formation of HCA. In addition, the peak intensity of Si was reduced as the immersion time increased, which can be attributed to an increase in the amount of HCA developed on the surface of the coating.

On the other hand, FTIR analysis of the coatings was performed, and FTIR spectra for 1, 7 and 14 days of immersion are displayed in figure 12. In the spectra, absorption bands of PO_4^{3-} at 560 and 605 cm^{-1}, which correspond to P–O bending, and at 1050 cm^{-1} associated to P–O stretching can be appreciated. These peaks can be easily distinguished at 7 days and their intensity grows at 14 days. Other absorption bands were identified, two corresponding to carbonate group or CO_3^{2-} (at 870 and 1400 cm^{-1}) and one at 800 cm^{-1} which relates to Si–O stretching. Although the P–O bands at 560 and 605 cm^{-1} are used to corroborate the presence of HA or HCA [33], they were not characteristic of both materials, they just indicated the presence of orthophosphate lattices [43].

Therefore, the presence of HCA was assessed by XRD (Figure 13). The resulting patterns confirmed the nucleation and growing of HCA on the coatings surface, showing sharp peaks at 2θ of 26 and 32 degrees just for 1 immersion day. These peaks were preserved for 7 and 14 days, while the crystalline phases (combeite and tricalcium silicate) disappeared as the incubation time increased. Moreover, the dissolution of the glass agglomerates observed from SEM surface micrographs could be also demonstrated by observing the XRD patterns, since by increasing the incubation time, a decrease in the intensity of the amorphous phase (between 2θ of 15 and 25 degrees) as well as an increase in intensity of the peaks corresponding to anatase (related to the bond coat as set out above) occurred. The main peak

of calcium carbonate was also detected in the XRD patterns, but this compound precipitated from the SBF on the surface of the coating since the incubation medium was saturated [44], and its intensity decreased as the soaking time increased.

4. Conclusions

Bioactive glass solution feedstocks were developed with different amounts of catalyst to hydrolyse the alkoxides. As–prepared, all feedstock solutions were suitable to be injected into the plasma torch as they had low viscosity at higher shear rates. In addition, their thermal behaviour made them suitable to obtain bioactive glass coatings. However, higher amount of catalyst resulted in a non–stable feedstock over time because the solution gelation quickly occurred.

The sol containing 0.2 M of catalyst was the only one that allowed to deposit a coating. Different coatings were deposited from this feedstock under two spraying distances and argon flow rates, observing that both variables exerted a great effect on the final coating microstructure. The best quality coating was developed under the shorter spraying distance and the higher argon flow rate. The as–sprayed coating revealed a dense and homogeneous microstructure composed of two zones typical of liquid feedstocks (a first layer of fine drops and a top layer of glass agglomerates) exhibiting a very high surface area. Scratch tests was carried in comparison with APS and SPS coating counterparts. The findings showed that SPPS coating possessed good mechanical (adhesion and cohesion) performance. In vitro test of this coating confirmed its good bioactivity. In addition, it was observed that the ability of the coating to react with the biological fluid was highly influenced by the microstructure.

Based on the obtained results, it can be concluded that is possible to deposit bioactive glass coatings by SPPS with a dense microstructure, good adhesion and suitability to react with biological fluids. However, more work is already in progress with the aim of further improvement of feedstock stability, the coating adherence as well as of eliminating the crystalline phase formation of. Moreover, doping elements will be also introduced in order to improve the biological response of the developed coatings.

Acknowledgements

The authors of the present work thank Universitat Jaume I of Castellón the support provided in funding action 3.1. of the Research Promotion Plan (PREDOC/2015/50) and The European Virtual Institute on Knowledge–based Multifunctional Materials ASBL (KMM–VIN) for the KMM–VIN Research Fellowship (call 2016).

References

[1] J.A. Juhasz, S.M. Best, Bioactive ceramics: processing, structures and properties, J. Mater. Sci. 47 (2012) 610–624.

[2] V.J. Shirtliff, L.L. Hench, Bioactive materials for tissue engineering, regeneration and repair, J. Mater. Sci. 38 (2003) 4697–4707.

[3] M. Akao, H. Aoki, K. Kato, Mechanical properties of sintered hydroxyapatite for prosthetic applications, J. Mater. Sci. 16 (1981) 809–812.

[4] K.A. Hiller, W. Buchalla, I. Grillmeier, C. Neubauer, G. Schmalz, In vitro effects of hydroxyapatite containing toothpastes on dentin permeability after multiple applications and ageing, Sci. Rep. 8 (2018) 4888–4900.

[5] D.M. Devine, E. Hoctor, J.S. Hayes, E. Sheehan, C.H. Evans, Extended release of proteins following encapsulation in hydroxyapatite/chitosan composite scaffolds for bone tissue engineering applications, Mat. Sci. Eng. C 84 (2018) 281–289.

[6] J.R. Jones, Review of bioactive glass: From Hench to hybrids, Acta Biomater. 23 (2015) 53–82.

[7] A.R. Boccaccini, M. Erol, W.J. Stark, D. Mohn, Z. Hong, J.F. Mano, Polymer/bioactive glass nanocomposites for biomedical applications: A review, Compos. Sci. Technol. 70 (2010) 1764–1776.

[8] E. Cañas, M. Vicent, M.J. Orts, E. Sánchez, Bioactive glass coatings by suspension plasma spraying from glycolether–based solvent feedstock, Surf. Coat. Technol. 318 (2017) 190–197.

[9] J.A. Helsen, J. Proost, J. Schrooten, G. Timmermans, E. Brauns, J. Vanderstraeten, Glasses and bioglasses: synthesis and coatings, J. Eur. Ceram. Soc. 17 (1997) 147–152.

[10] P. Stoor, E. Söderling, J.I. Salonen, Antibacterial effects of a bioactive glass paste on oral microorganisms, Acta Odont. Scan. 56 (1998) 161–165.

[11] A.A. Gorustovich, C. Perio, J.A. Roether, A.R. Boccaccini, Effect of Bioactive Glasses on Angiogenesis: A Review of In Vitro and In Vivo Evidences, Tissue Eng. B 16 (2010) 199–207.

[12] W. Cao, L. Hench, Bioactive materials, Ceram. Inter. 22 (1996) 493–507.

[13] A. Sola, D. Bellucci, V. Cannillo, A. Cattini, Bioactive glass coatings: a review, Surf. Eng. 27 (2011) 560–572.

[14] F. Baino, E. Verne, Glass–based coatings on biomedical implants: a state–of–the–art review, Biomed. Glasses 3 (2017) 1–17.

[15] J.R. Jones, A.G. Clare, Bio–glasses: An introduction (first ed.), John Wiley & Sons, Great Britain (2012).

[16] V. Cannillo, A. Sola, Different approaches to produce coatings with bioactive glasses: Enamelling vs plasma spraying, J. Eur. Ceram. Soc. 30 (2010) 2031–2039.

[17] V. Cannillo, A. Sola, Potassium–based composition for a bioactive glass, Ceram. Inter. 35 (2009) 3389–3393.

[18] C.C. Mardare, A.I. Mardare, J.R.F. Fernandes, E. Joanni, S.C.A. Pina, M.H.V. Fernandes, R.N. Correia, Deposition of bioactive glass–ceramic thin–films by RF magnetron sputtering, J. Eur. Ceram. Soc. 23 (2003) 1027–1030.

[19] P. González, J. Serra, S. Liste, S. Chiussi, B. León, M.P. Amor, J.M. Fernández, A.R.A. López, F.M.V. Feria, New biomorphic SiC ceramics coated with bioactive glass for biomedical applications, Biomater. 24 (2003) 4827–4832.

[20] E. Cañas, M. Vicent, E. Bannier, P. Carpio, M.J. Orts, E. Sánchez, Effect of particle size on processing of bioactive glass powder for atmospheric plasma spraying, J. Eur. Ceram. Soc. 36 (2016) 837– 845.

[21] J. Zhong, D.C. Greenspan, Processing and properties of sol–gel bioactive glasses, J. Biomed. Mater. Res. Appl. Biomater. 53 (2000) 694–701.

[22] M. Monsalve, H. Ageorges, E. Lopez, F. Vargas, F. Bolivar, Bioactivity and mechanical properties of plasma–sprayed coatings of bioglass powders, Surf. Coat. Technol. 220 (2013) 60 – 66.

[23] A. Killinger, R. Gadow, G. Mauer, A. Guignard, R. Vassen, D. Stöver, Review of new developments in suspension and solution precursor thermal spray processes, J. Therm. Spray Technol. 20 (2011) 677–695.

[24] I. Rocnakova, K. Slamecka, E.B. Montufar, M. Remesova, L. Dyckova, A. Brinek, D. Jech, K Dvorak, L. Celko, J. Kaiser, Deposition of hydroxyapatite and tricalcium phosphate coatings by suspension plasma spraying: effects of torch speed, J. Eur. Ceram. Soc. https://doi.org/10.1016/j.jeurceramsoc.2018.08.007.

[25] X. Ma, P. Ruggiero, Practical Aspects of Suspension Plasma Spray for Thermal Barrier Coatings on Potential Gas Turbine Components, J. Therm. Spray Technol. 27 (2018) 591–602.

[26] O.P. Solonenko, Y. Ando, H. Nishiyama, D. Kindole, A.V. Smirnov, A.A. Golovin, S. Uehara, T. Nakajima, Synthesis of thick photocatalytic titania surface layers by solution plasma spraying and subsequent treatment by pulsed laminar plasma jet, Surf. Coat. Technol. 333 (2018) 39–51.

[27] P. Xu, L. Pershin, J. Mostaghimi, T.W. Coyle, Efficient one–step fabrication of ceramic superhydrophobic coatings by solution precursor plasma spray, Mat. Lett. 211 (2018) 24–27.

[28] G. Bolelli, D. Bellucci, V. Cannillo, R. Gadow, A. Killinger, L. Lusvarghi, P. Müller, A. Sola, Comparison between suspension plasma sprayed and high velocity suspension flame sprayed bioactive coatings, Surf. Coat. Technol. 280 (2015) 232–249.

[29] A. Cattini, L. Latka, D. Bellucci, G. Bolelli, A. Sola, L. Lusvarghi, L. Pawlowski, V. Cannillo, Suspension plasma sprayed bioactive glass coatings: effects of processing on microstructure, mechanical properties and in–vitro behaviour, Surf. Coat. Technol. 220 (2013) 52–59.

[30] E. Cañas, M.J. Orts, A.R. Boccaccini, E. Sánchez, Solution Precursor Plasma Spraying (SPPS): A novel and simple process to obtain bioactive glass coatings, Mat. Lett. 223 (2018) 198–202.

[31] Q.Z. Chen, Y. Li, L.Y. Jin, J.M.W. Quinn, P.A. Komesaroff, A new sol–gel process for producing Na_2O–containing bioactive glass ceramics, Acta Biomater. 6 (2010) 4143–4153.

[32] J. Faure, R. Drevet, A. Lamelle, N.B. Jaber, A. Tara, H. El Btaouri, H. Benhayoune, A new sol–gel synthesis of 45S5 bioactive glass using an organic acid as catalyst, Mater. Sci. Eng. C 47 (2015) 407–412.

[33] H. Pirayesh, J.A. Nychka, Sol–gel synthesis of bioactive glass–ceramic 45S5 and its in vitro dissolution and mineralization behavior, J. Am. Ceram. Soc. 96 (2013) 1643–1650.

[34] C.J. Brinker, G.W. Scherer, Sol–gel science. The physics and chemistry of sol–gel processing (first ed.), Academic Press, USA (1990).

[35] Y. Castro, A. Durán, R. Moreno, B. Ferrari, Thick sol–gel coatings produced by electrophoretic deposition, Adv. Mater. 14 (2002) 505–508.

[36] R.T. Candidato Jr., P. Sokolowski, L. Pawlowski, G. Lecomte–Nana, C. Constantinescu, A. Denoirjean, Development of hydroxyapatite coatings by solution precursor plasma spray process and their microstructural characterization, Surf. Coat. Technol. 318 (2017) 39–49.

[37] M. Vicent, E. Bannier, P. Carpio, E. Rayón, R. Benavente, M.D. Salvador, E. Sánchez, Effect of the initial particle size distribution on the properties of suspension plasma sprayed Al_2O_3–TiO_2 coatings, Surf. Coat. Technol. 268 (2015) 209–215.

[38] P. Carpio, E. Bannier, M.D. Salvador, A. Borrell, R. Moreno, E. Sánchez, Effect of particle size distribution of suspension feedstock on the microstructure and mechanical properties of suspension plasma spraying YSZ coatings, Surf. Coat. Technol. 268 (2015) 293–297.

[39] G. Goller, The effect of bond coat on mechanical properties of plasma sprayed bioglass–titanium coatings, Ceram. Int. 30 (2004) 351–355.

[40] R.T. Candidato Jr., P. Sokolowski, L. Pawlowski, A. Denoirjean, Preliminary study of hydroxyapatite coatings synthesis using solution precursor plasma spraying, Surf. Coat. Technol. 277 (2015) 242–250.

[41] M. Khan, N. Hu, L. Zhenhua, Y. Wang, Z. Yi, Influence of solution–precursor plasma spray (SPPS) processing parameters on the mechanical and thermodynamic properties of 8YSZ, Ceram. Inter. 44 (2018) 7794–7798.

[42] R. Jaworski, L. Pawlowski, F. Roudet, S. Kozerski, F. Petit, Characterization of mechanical properties of suspension plasma sprayed TiO_2 coatings using scratch test, Surf. Coat. Technol. 202 (2008) 2644–2653.

[43] A.L.B. Maçon, T.B. Kim, E.M. Valliant, K. Goetschius, R.K. Brow, D.E. Day, A. Hoppe, A.R. Boccaccini, I.Y. Kim, C. Ohtsuki, T. Kokubo, A. Osaka, M. Vallet–Regí, D. Arcos, L. Fraile, A.J. Salinas, A.V. Teixeira, Y. Vueva, R.M. Almeida, M. Miola, C.

Vitale–Brovarone, E. Verné, W. Höland, J.R. Jones, A unified in vitro evaluation for apatite–forming ability of bioactive glasses and their variants, J. Mater. Sci. Mater. Med. 26 (2015) 115–124.

[44] T. Kokubo, H. Takadama, How useful is SBF in predicting in vivo bone bioactivity?, Biomater. 27 (2006) 2907–2915.

[45] V. Carnicer, C. Alcazar, E. Sánchez, R. Moreno, Aqueous suspension processing of multicomponent submicronic Y–TZP/Al_2O_3/SiC particles for suspension plasma spraying, J. Eur. Ceram. Soc. 38 (2018) 2430–2439.

[46] L. Xie, X. Ma, A. Ozturk, E.H. Jordan, N.P. Padture, B.M. Cetegen, D.T. Xiao, M. Gell, Processing parameter effects on solution precursor plasma spray process spray patterns, Surf. Coat. Technol. 183 (2004) 51–61.

[47] M. Gell, E.H. Jordan, M. Teicholz, B.M. Cetegen, N.P. Padture, L. Xie, D. Chen, X. Ma, J. Roth, Thermal Barrier Coatings Made by the Solution Precursor Plasma Spray Process, J. Therm. Spray Technol. 17 (2008) 124–135.

[48] Z. Yu, H. Moussa, M. Liu, R. Schneider, M. Moliere, H. Liao, Solution precursor plasma spray process as an alternative rapid one–step route for the development of hierarchical ZnO films for improved photocatalytic degradation, Ceram. Inter. 44 (2018) 2085–2092.

Table 1 Plasma spraying parameters used

Spraying parameters	**TiO_2 bond coat (APS)**	**Bioactive glass top coat (SPPS)**
Ar (slpm)*	38	25–45
H_2 (slpm)*	14	15
Intensity (A)	600	600
Spraying distance (mm)	120	70–110
Scan velocity (mm s^{-1})	1000	1250
Feed rate	45 g/min	33 ml/min

**Standard litres per minute*

Table 2. Solution feedstock composition

Oxide (wt%)	**SiO_2**	**CaO**	**Na_2O**	**P_2O_5**
Nominal 45S5 glass	45.0	24.5	24.5	6.0
Solution feedstock	46.0	23.3	25.5	5.3

Table 3. Experiment grid resulting from the combination of each modified parameter

Number of experiment	Spraying distance (mm)	Argon flow rate (slpm)
1	70	25
2	110	25
3	70	45
4	110	45

Table 4. Mechanical properties of plasma sprayed bioactive glass coatings

Tested coating	Critical load, L_c (N)	HS_P (GPa)
Atmospheric plasma spraying	10	0.64
Suspension plasma spraying	1	0.06
Solution precursor plasma spraying	5	1.27

Figure Captions

Figure 1. DTA–TG/DTG curves of each solution feedstock. a) DTA for the 0.2 M sol. b) TG/DTG for the 0.2 M sol. c) DTA for the 0.5 M sol. d) TG/DTG for the 0.5 M sol. e) DTA for the 1 M sol. f) TG/DTG for the 1 M sol

Figure 2. Flow curve of the solution feedstocks with different amounts of catalyst

Figure 3. Stability with time (gelation time) for each solution based on their viscosity values

Figure 4. Surface micrographs of coatings deposited with the solution containing 0.2 M of catalyst. a) and e) run 1. b) and f) run 2. c) and g) run 3. d) and h) run 4

Figure 5. Cross–section micrographs of the unique adhered coating (run 1)

Figure 6. XRD pattern of the as–sprayed coating (run 1)

Figure 7. Example of the scratches performed on the coatings. a) Atmospheric plasma sprayed coating (from [20]). b) Suspension plasma sprayed coating (from [8]). c) Solution precursor plasma sprayed coating (from run 1)

Figure 8. Penetration depth curve of the scratches performed in each coating. a) Atmospheric plasma sprayed coating (from [20]). b) Suspension plasma sprayed coating (from [8]). c) Solution precursor plasma sprayed coating (from run 1)

Figure 9. pH of the SBF (diamond dots) and SBF containing the coatings (circle dots) for each soaking time

Figure 10. Surface micrographs of the soaked coatings. a), b) and c) 1 day of immersion. e), f) and g) corresponds to 7 days of immersion. h), i) and j) for 14 days

Figure 11. EDX patterns of the sprayed coating. a) As–sprayed. b) 1 day of immersion in SBF. c) 7 days of immersion in SBF. d) 14 days of immersion in SBF

Figure 12. FTIR of the coatings after being soaked for 1, 7 and 14 days

Figure 13. XRD patterns of the coatings immersed in SBF after 1, 7 and 14 days

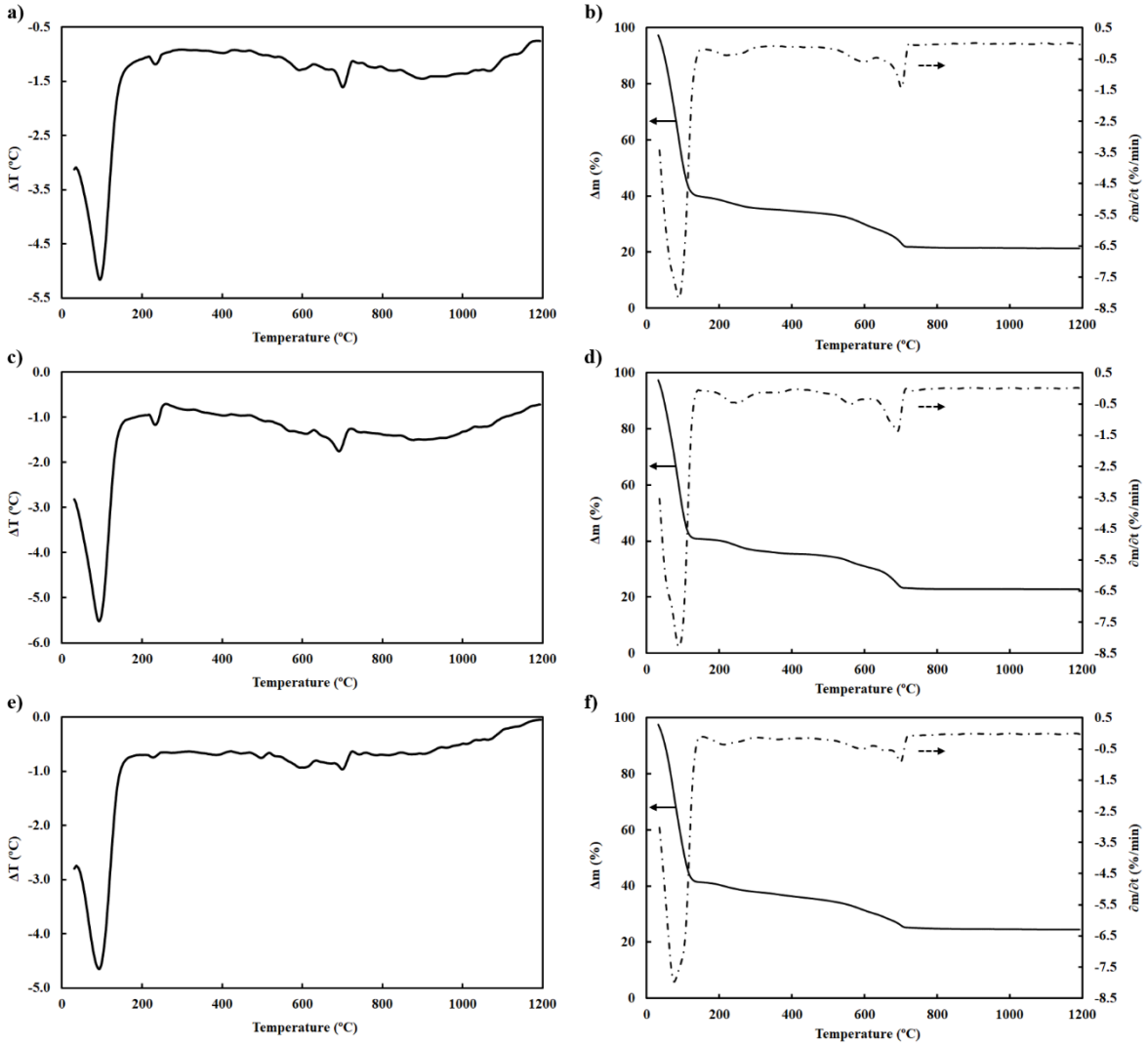
a)
ΔT (°C)
Temperature (°C)
b)
Δm (%)
∂m/∂t (%/min)
Temperature (°C)
c)
ΔT (°C)
Temperature (°C)
d)
Δm (%)
∂m/∂t (%/min)
Temperature (°C)
e)
ΔT (°C)
Temperature (°C)
f)
Δm (%)
∂m/∂t (%/min)
Temperature (°C)

Figure 1

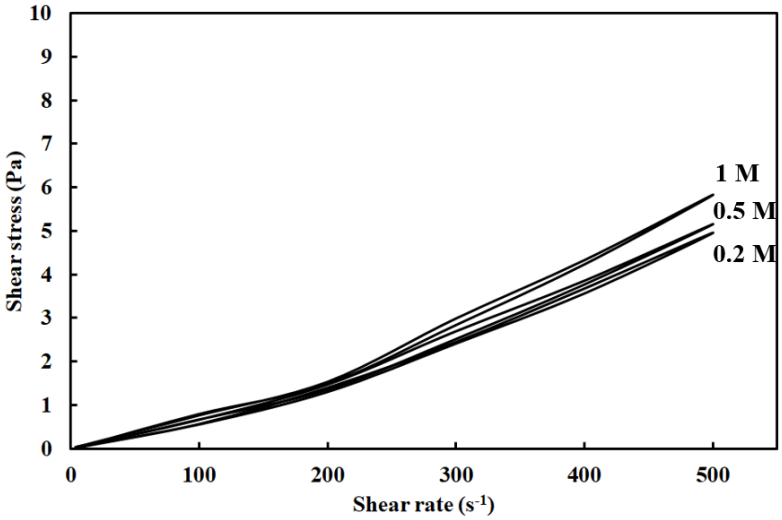
Shear stress (Pa)
Shear rate (s-1)
1 M
0.5 M
0.2 M
0
1
2
3
4
5
6
7
8
9
10
0
100
200
300
400
500

Figure 2

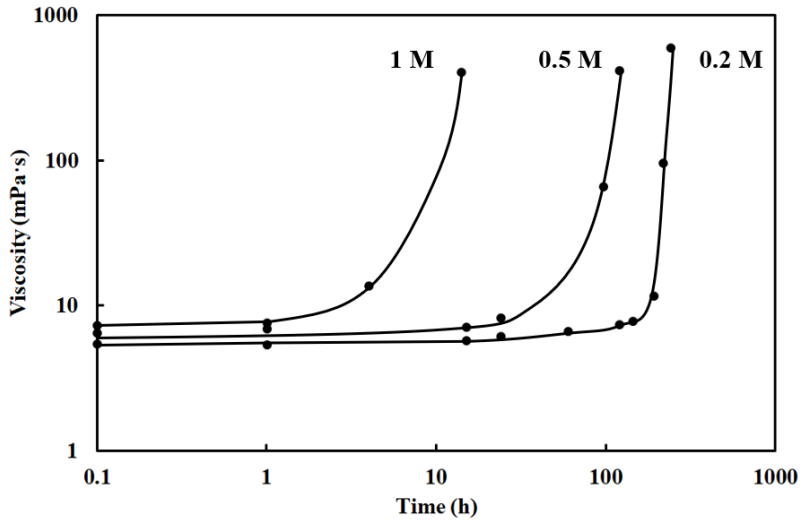

Figure 3

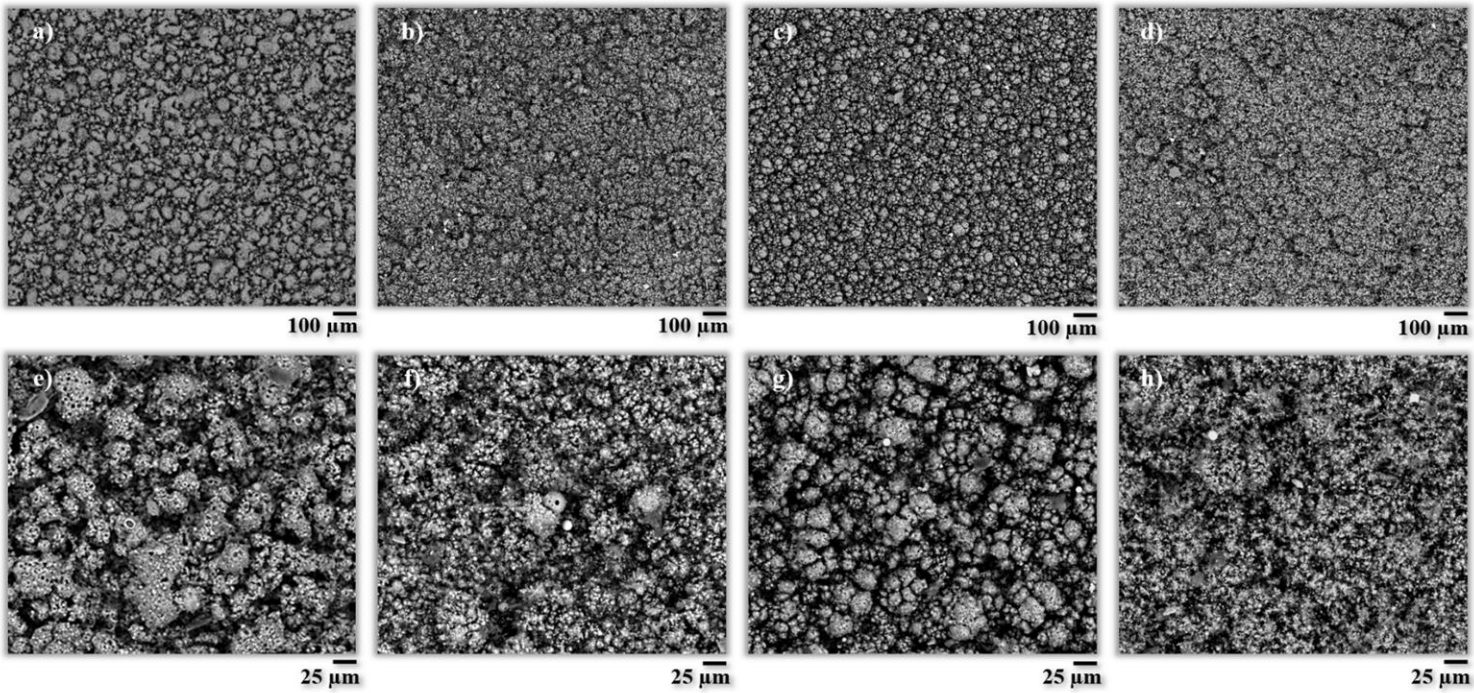

Figure 4

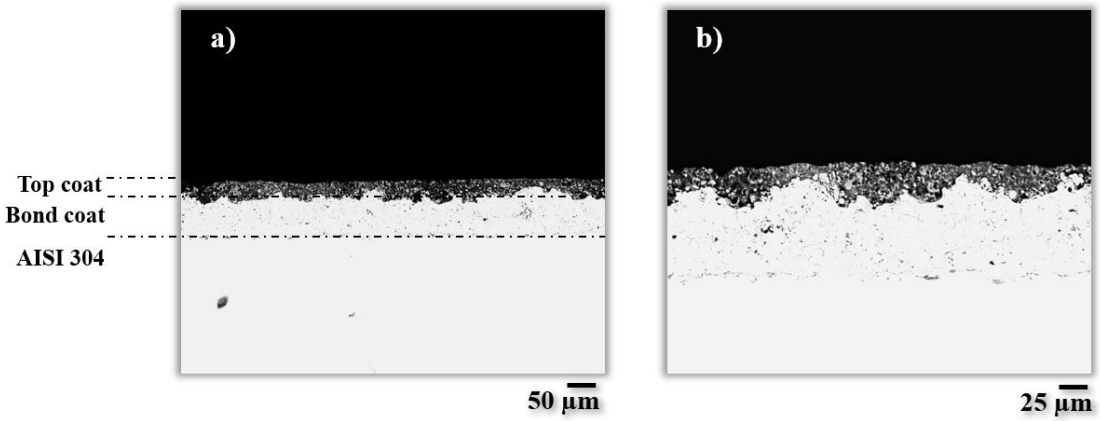

Figure 5

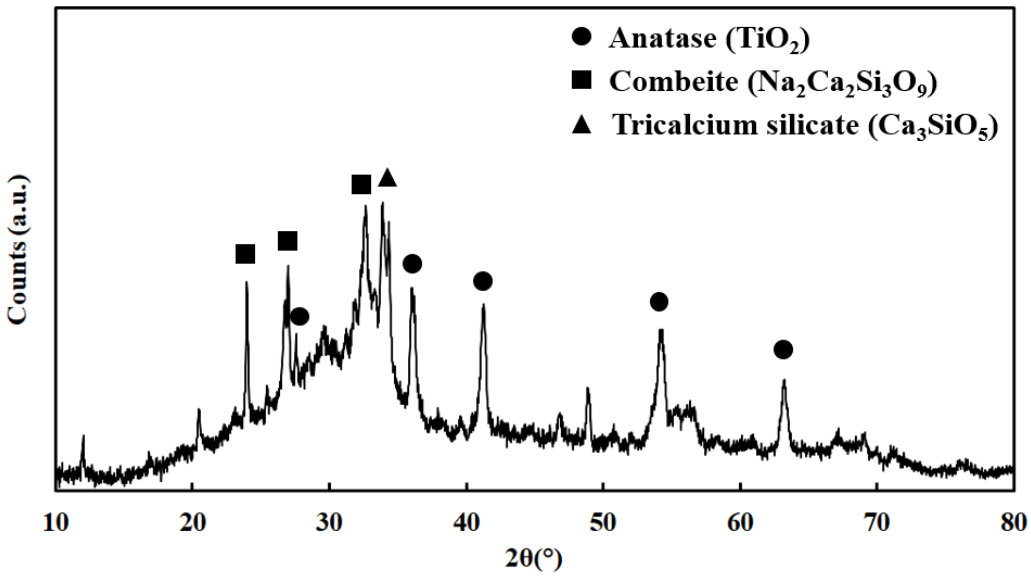
Anatase (TiO_2)
Combeite ($Na_2Ca_2Si_3O_9$)
Tricalcium silicate (Ca_3SiO_5)
Counts (a.u.)
10
20
30
40
50
60
70
80
2θ(°)

Figure 6

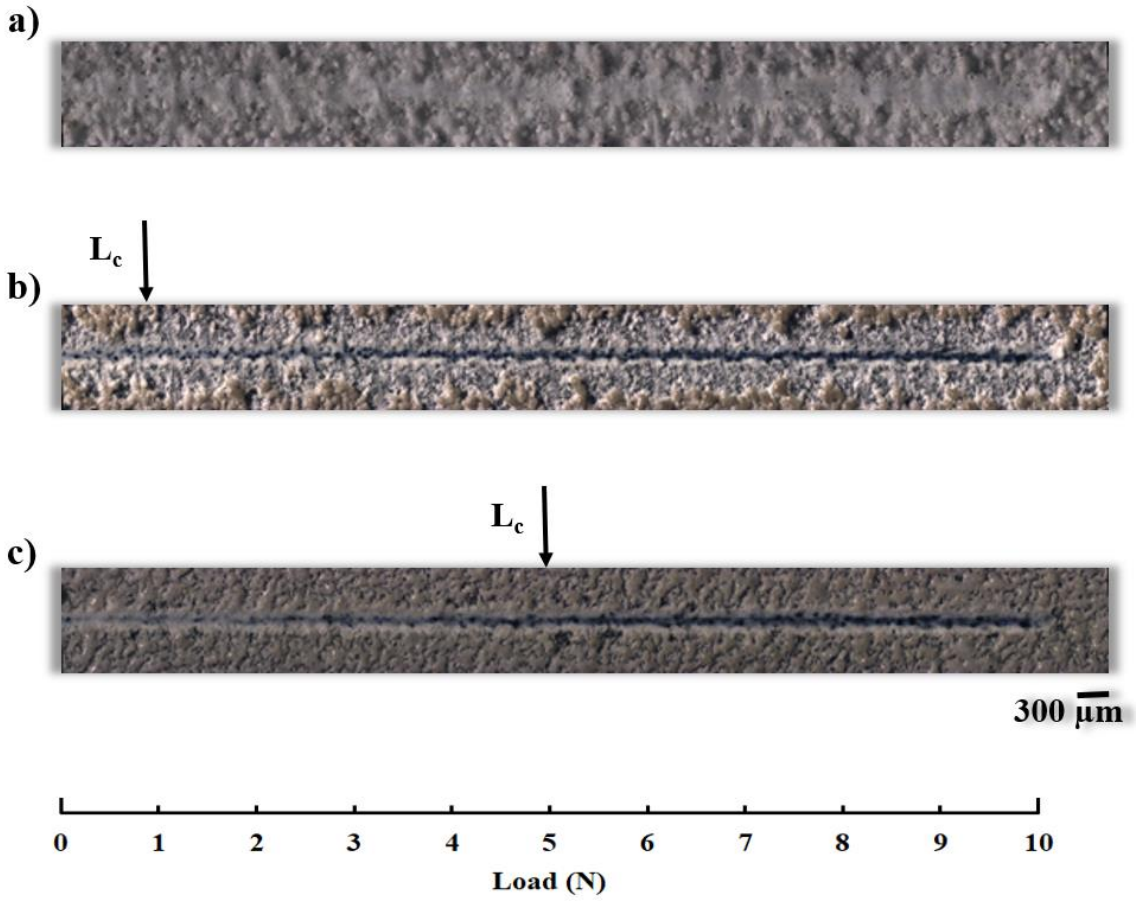

Figure 7

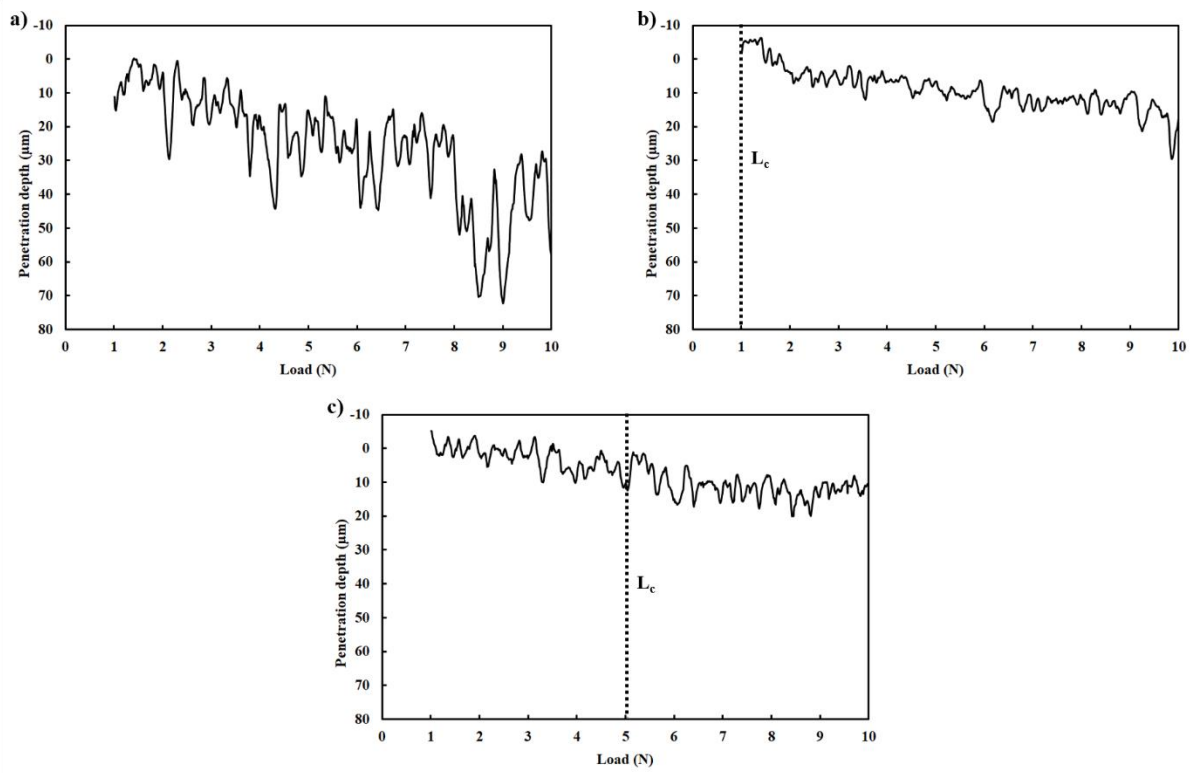

Figure 8

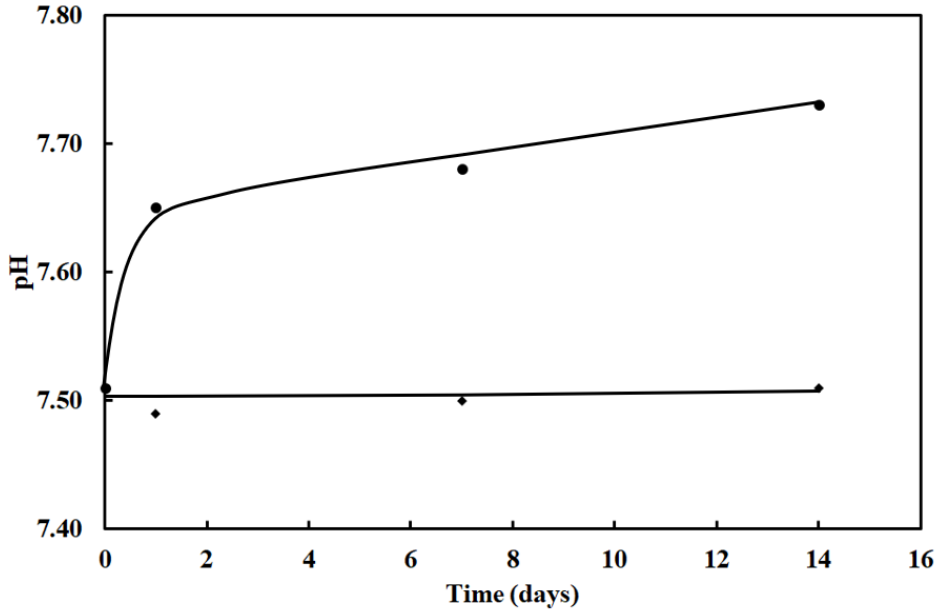

Figure 9

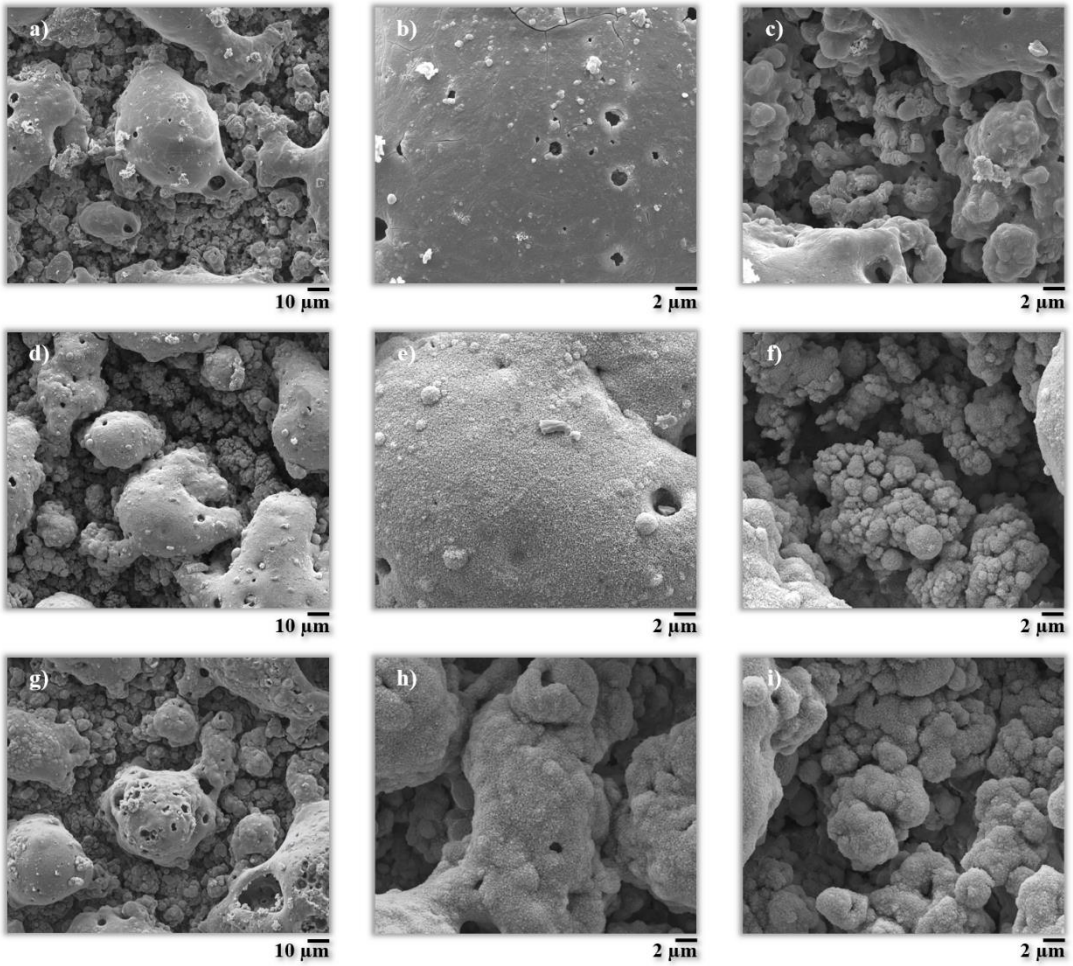

Figure 10

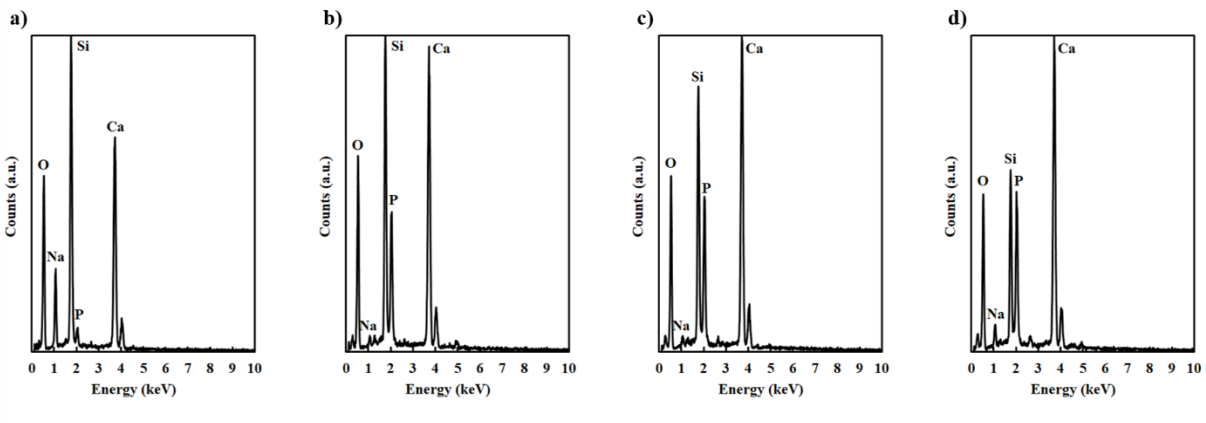

Figure 11

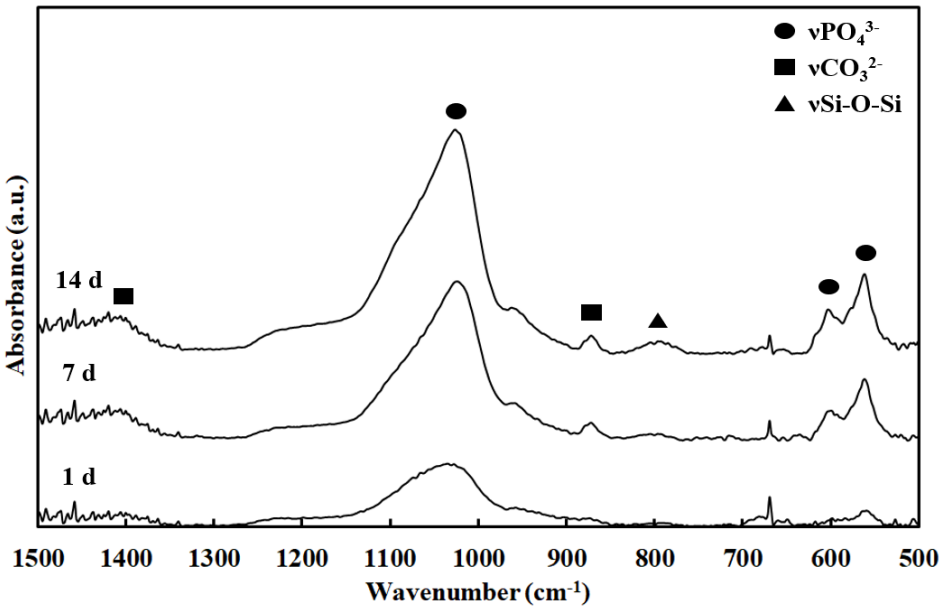
νPO4 3-
νCO3 2-
νSi-O-Si
Absorbance (a.u.)
14 d
7 d
1 d
1500
1400
1300
1200
1100
1000
900
800
700
600
500
Wavenumber (cm-1)

Figure 12

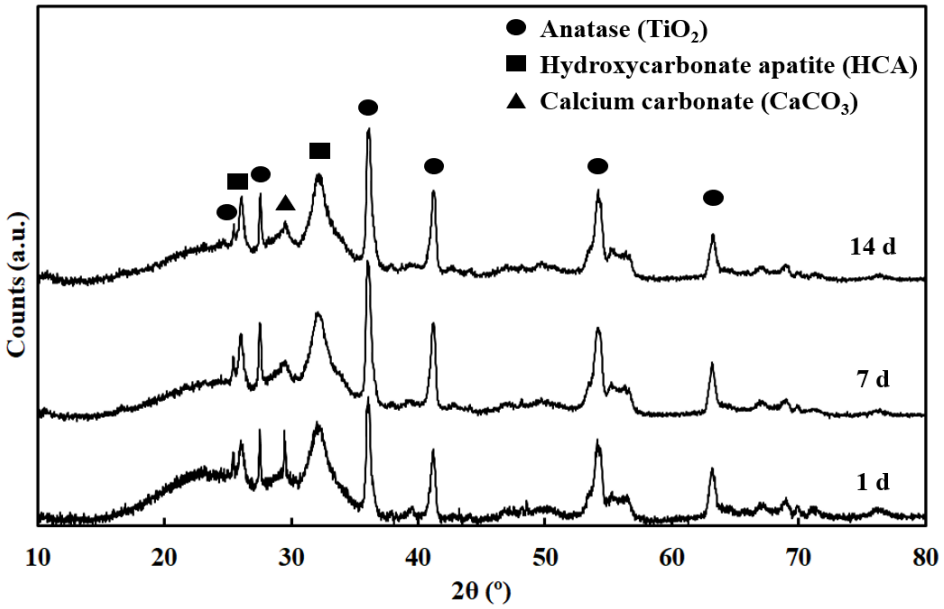
Anatase (TiO_2)
Hydroxycarbonate apatite (HCA)
Calcium carbonate ($CaCO_3$)
14 d
7 d
1 d
Counts (a.u.)
10
20
30
40
50
60
70
80
2θ (°)

Figure 13